Article

Piper chaba Stem Extract Facilitated the Synthesis of Iron Oxide Nanoparticles as an Adsorbent to Remove Congo Red Dye

Sangjukta Yesmin, Md. Mahiuddin, A. B. M. Nazmul Islam, Kaykobad Md Rezaul Karim, Prianka Saha, Md. Abu Rayhan Khan, and Habib Md. Ahsan*
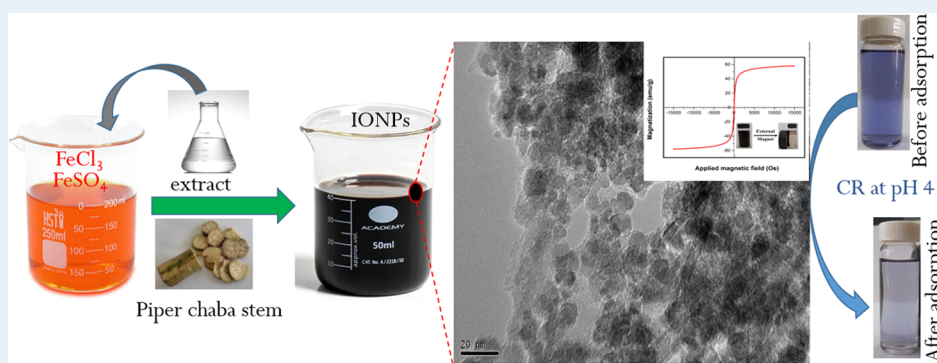
Cite This: ACS Omega 2024, 9, 10727−10737

Read Online

ACCESS | Metrics & More | Article Recommendations

ABSTRACT: In this study, a straightforward, eco-friendly, and facile method for synthesizing iron oxide nanoparticles (IONPs) utilizing *Piper chaba* steam extract as a reducing and stabilizing agent has been demonstrated. The formation of stable IONPs coated with organic moieties was confirmed from UV−vis, FTIR, and EDX spectroscopy and DLS analysis. The produced IONPs are sufficiently crystalline to be superparamagnetic having a saturation magnetization value of 58 emu/g, and their spherical form and size of 9 nm were verified by XRD, VSM, SEM, and TEM investigations. In addition, the synthesized IONPs exhibited notable effectiveness in the removal of Congo Red (CR) dye with a maximum adsorption capacity of 88 mg/g. The adsorption kinetics followed pseudo-second-order kinetics, meaning the adsorption of CR on IONPs is mostly controlled by chemisorption. The adsorption isotherms of CR on the surface of IONPs follow the Langmuir isotherm model, indicating the monolayer adsorption on the homogeneous surface of IONPs through adsorbate−adsorbent interaction. The IONPs have revealed good potential for their reusability, with the adsorption efficiency remaining at about 85% after five adsorption−desorption cycles. The large-scale, safe, and cost-effective manufacturing of IONPs is made possible by this environmentally friendly process.

1. INTRODUCTION

Nanotechnology deals with the observation, measurement, manipulation, manufacture, and utilization of an object on an atomic or molecular scale, typically within the range of 1−100 nm. These nanoscopic materials' physical, chemical, optical, and electrical properties are greatly influenced by their size, shape, and surface morphology. The most important and fascinating characteristic of these tiny objects is their high surface area to volume ratio, which endorse the nanomaterials to be widely used in many areas of engineering and material science as well as electronics, optics, medicine, mechanics, catalysis, and biotechnology.[1−5] Metal oxide nanoparticles are significant members of the nanomaterials family and usually have enhanced chemical, thermal, optical, electrical, or magnetic properties, making them appropriate for application in electronic and biomedical devices as well as pigments, coatings, and inks as well as catalysis.[4,6−11] Particularly, iron oxide nanoparticles (IONPs) have drawn a lot of interest because of a variety of distinctive magnetic properties, such as superparamagnetic properties, high coercivity, low Curie temperature, high magnetic susceptibility, etc. Due to these, magnetic NPs are of great interest to researchers in a range of fields, including magnetic fluids, data storage, catalysis, and bioapplications.[9,10,12−15]
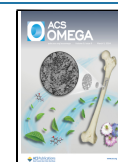
Many methods, such as the template-assisted synthesis method, hydrothermal synthesis, vapor−solid growth techniques, sol−gel process, chemical coprecipitation, thermal decomposition, and ultraviolet radiation and aerosol, have

been used in a huge number of studies on the development of synthetic methods to produce IONPs.[9,10,12,13,15−17] The synthesis process ought to be able to reduce toxicity and increase the biocompatibility of the nanoparticles. In addition to all of the ways discussed above, research is also being done on IONPs produced biologically, such as by quick and simple plant-mediated synthesis and microorganism-based processes.[18−20] In addition to these characteristics, the duration of the operation and the requirement for aseptic settings are other constraints for microorganism-based procedures. IONPs have recently been produced using a variety of plant-mediated processes because extraction and separation are simple to scale up for the large-scale synthesis of nanoparticles.[15,19,21−33] Additionally, the environmentally friendly IONPs have been extensively used as an antibacterial agent,[21,25,28] an adsorbent material for the removal of organic dyes[27,31−33] and heavy metal ions,[22,24] organic dye degradation catalysts,[25,29,34] and in many other applications. This motivates us to concentrate our research on the environmentally friendly synthesis of IONPs and their amazing applications.

Piper chaba, also known as chui jhal or choi jhal, is a common plant that is a member of the Piperaceae family. In South and Southeast Asia, it is a widely available, inexpensive, and edible plant. Beyond only eating, it has a variety of uses, including analgesic, antibacterial, antioxidant, and hypotensive ones. There are many different substances in *P chaba*, but alkaloids and lignans, such as piperine, kusunokinin, and piplartine are the most common.[35−38] These phytochemicals have demonstrated their reducing and stabilizing ability to reduce silver ions to form well-stable silver nanoparticles.[39] We believe that similar to silver nanoparticles, *P. chaba* will also exhibit the same potential in the case of the formation of IONPs, which has not been reported yet.

Organic pollutants are still being discharged as effluents from many sectors and are hurting the environment, particularly in water. These pollutants are bad for both human and animal health since they can lead to a variety of illnesses including poisoning of the central nervous system, skin rashes, kidney and liver damage, and blood abnormalities. The capacity of some processes, such as membrane separation, coagulation, oxidative remediation, and adsorption, to remove dyes from an aqueous medium makes them stand out.[27,31,34,40,41] Since there is a strong correlation between the quantity of surface area and the volume of the adsorbent, nanotechnology is effectively used in adsorption to purify water, and different nanomaterials have been promisingly used as adsorbents.[29,42−45] This results in a significant cost reduction that is directly connected to the lesser amount of adsorbent used. IONPs are one of the most often used nanomaterials because of how simple they are to synthesize and how many different chemicals they can uptake on their surface or in combination with other adsorbents.[20,31−34]

In this study, magnetic IONPs were synthesized easily and sustainably using the stem extract of *P. Chaba* as a green reducing and stabilizing agent. Additionally, using Congo red as a model dye, we examined the dye removal effectiveness of the green synthesized IONPs to assess their potential as adsorbents. The large-scale production of IONPs for the removal of organic contaminants in wastewater treatment may find this research work to be remarkable.

2. RESULTS AND DISCUSSION

2.1. Characterization of Nanoparticles. IONPs were synthesized by coprecipitation of iron salts in an alkaline medium using *P. Chaba* plant extract as the reducing and capping agents. Visual observation of color change by the naked eye is one of the important approaches to forecasting the formation of distinct metal nanoparticles. Here, the formation of IONPs was also anticipated by changing the color of the reaction mixture from brown to black (the inset image in Figure 1), which was synthesized by reacting ferric
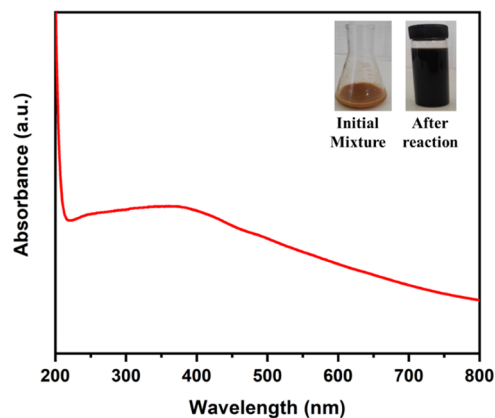

Figure 1. Optical image and UV−vis spectrum of IONPs synthesized using *P. Chaba* stem extract (conditions: 80 °C and 30 min).

chloride and ferrous sulfate with the stem extract of *P. Chaba* at 80 °C for 30 min. By displaying the surface plasmon resonance (SPR) band at the distinctive location, UV−vis spectroscopy analysis was thought of as a key technique to confirm the formation of various metal nanoparticles. As a result, a broad absorption band serving as a representative SPR band of IONPs at 390 nm (Figure 1), which is the characteristic SPR region of IONPs, was demonstrated, confirming the construction of the IONPs utilizing the stem extract of *P. chaba*.[24]

Powder X-ray diffraction analysis is key to determining the phase and crystalline structures of the nanoparticles. The XRD pattern of green synthesized IONPs is shown in Figure 2. The pattern revealed six distinct diffraction peaks at $2\theta = 30.33$,
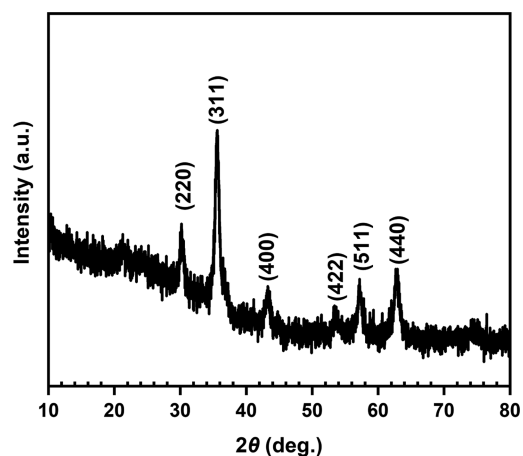

Figure 2. Powder XRD pattern of IONPs synthesized using *P. Chaba* stem extract (conditions: 80 °C and 30 min).

35.54, 43.31, 53.78, 57.10, and 62.71°. These peaks can be attributed to the lattice planes of (220), (311), (400), (422), (511), and (440), which are well indexed to the crystalline cubic phase of iron oxide (JCPDS card no. 019-0629). This indicates that the obtained IONPs are primarily composed of magnetite magnetic phases (Fe_3O_4), with the maghemite phase (γFe_2O_3) contributing very little.[30,46,47] The average crystallite size was calculated using the Scherrer formula

$$D = k\lambda/\beta \cos\theta \qquad (1)$$

where D represents the size of crystalline domains, k represents the dimensionless shape constant ($k = 1$ for spherical domains), λ represents the X-ray wavelength (0.1541 nm), β represents the full width at half-maximum, and θ represents the diffraction angle corresponding to the lattice plane. All of the mentioned lattice planes were used to calculate the average crystallite sizes, which were determined to be 6, 9, 10, 8, 6, and 9 nm for (220), (311), (400), (422), (511), and (440) planes, respectively. The values are very close to one another, suggesting that monodispersed IONPs were formed.

Analysis using vibrating sample magnetometry (VSM) is a crucial method for assessing the magnetic behavior of IONPs. Figure 3 shows the findings of the VSM study of greenly
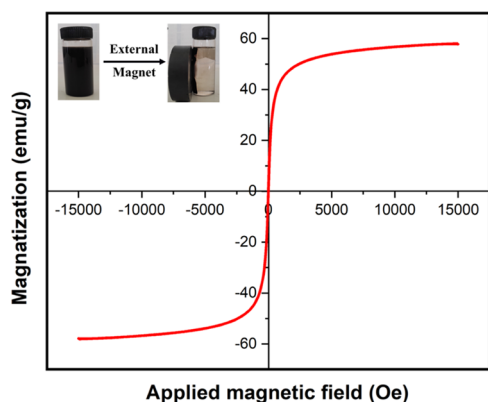

Figure 3. Optical image and magnetization curve of IONPs synthesized using *P. Chaba* stem extract (conditions: 80 °C and 30 min).

produced IONPs. The saturation magnetization (Ms) of the green synthesized IONPs was found to be 58 emu/g according to the magnetic hysteresis curve, whereas negligible coercivity (Hc) and no remanence magnetization (Mr) indicate that the synthesized IONPs by the *P. chaba* stem extract were superparamagnetic. By removing the resulting IONPs from the dispersion medium using an external magnet, the magnetic properties of the IONPs could also be seen visually (the inset image in Figure 3).

To confirm the presence of Fe_3O_4 and organic capping moieties on the IONPs' surface driven from the phytochemicals present in *P. chaba* stem extract, FTIR analysis was carried out. The FTIR spectra of the solid content of the *P. chaba* stem extract and IONPs that were prepared using the extract are shown in Figure 4. The FTIR spectrum of IONPs showed two peaks at 450 and 580 cm^{-1}, which were inconsistent with the FTIR spectrum of the solid content of the extract and suggested the presence of a Fe–O bond.[30,46] In addition, IONPs show a broad peak at 3447 cm^{-1} for O–H and N–H bond stretching, a strong signal at 1607 cm^{-1} for C=O stretching of the amide group in *P. Chaba*, and a minor signal
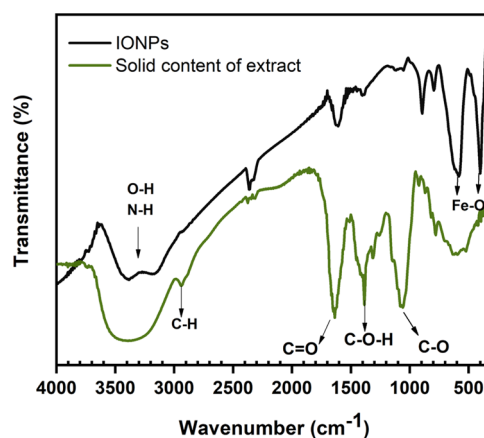

Figure 4. FTIR spectra of the solid content of *P. Chaba* stem extract and IONPs synthesized using *P. Chaba* stem extract (conditions: 80 °C and 30 min).

at 2925 cm^{-1} for C–H bond stretching.[48,49] Some additional bands were observed around 1300–1420 cm^{-1} assigned to C–O–H, O–C–H, and C–C–H bending, around 920–1110 cm^{-1} due to C–C and C–O stretching indicating the presence of polysaccharides, which are typically a significant component of plant sources, as capping molecules on the surface of IONPs. By comparing the FTIR spectrum of the green synthesized IONPs with the solid content of *P. Chaba* stem extract, it is simple to conclude that in addition to their reducing ability, some of the phytochemicals present in *P. Chaba* stem extract also possess promising capping abilities.

Electron microscopy analysis was carried out to investigate the size and morphology of the green synthesized IONPs. FE-SEM image (Figure 5a) shows that the particles are almost spherical with some rodlike structure in a highly aggregated form. Although high aggregation prevents the measurement of the particle sizes from the SEM image, we predicted the approximate size of the particles in the range of 26 to 50 nm. The stable water dispersibility of IONPs with an average hydrodynamic diameter (D_h) of 155 nm, which was examined by dynamic light scattering (DLS), suggested that such aggregation may have been caused by drying during sample preparation for SEM analysis (Figure 5b). The swollen phytochemicals adhering to the IONPs' surface and surrounding the hydration layer could be the reason for the larger D_h than was determined by SEM analysis. Silver nanoparticles synthesized using *P. chaba* stem extract showed a comparable difference too.[39]

We also performed TEM measurements to gain a better understanding of the size and morphology of the obtained IONPs. The TEM image (Figure 6a) reveals that the IONPs had an average 9 nm grain size and were spherical. Moreover, distinct lattice fringes that are visible in the HRTEM image (Figure 6b) support the formation of crystalline IONPs. The (311) and (220) planes correspond to an interplanar spacing of 0.258 and 0.278 nm, respectively.

To determine the elemental composition of the produced IONPs, EDX spectroscopy was used. The representative EDX spectrum of IONPs is shown in Figure 7, and the presence of the Fe (23%) and O (25%) signals indicates that the IONPs were formed, while the C (52%) signal may have arisen from the organic moieties that were present on the surface of IONPs originated from the *P. chaba* stem extract.
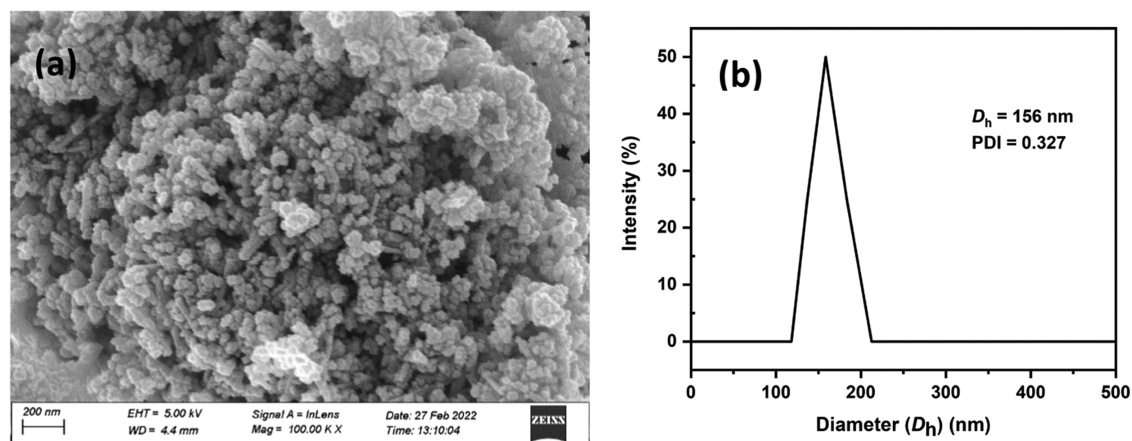
Figure 5. (a) Field emission scanning electron microscopy (FE-SEM) image and (b) DLS curve in the water of IONPs synthesized using *P. Chaba* stem extract (conditions: 80 °C and 30 min).
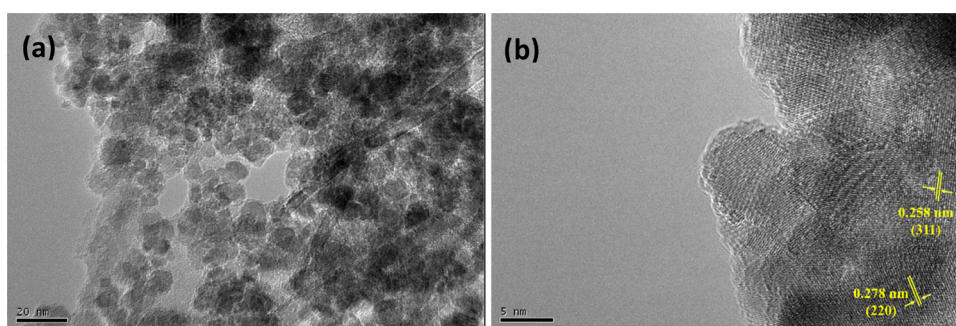

Figure 6. (a) TEM and (b) HRTEM images of IONPs synthesized using *P. Chaba* stem extract (conditions: 80 °C and 30 min).
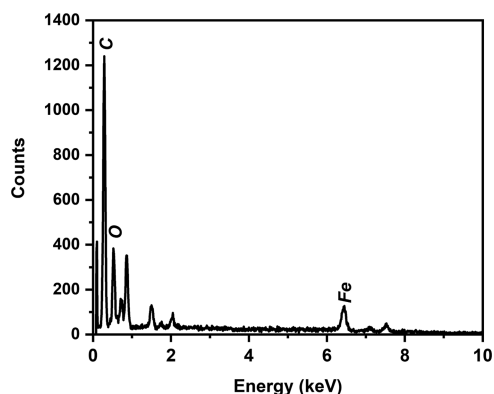

Figure 7. EDX spectrum of IONPs synthesized using *P. Chaba* stem extract (conditions: 80 °C and 30 min).
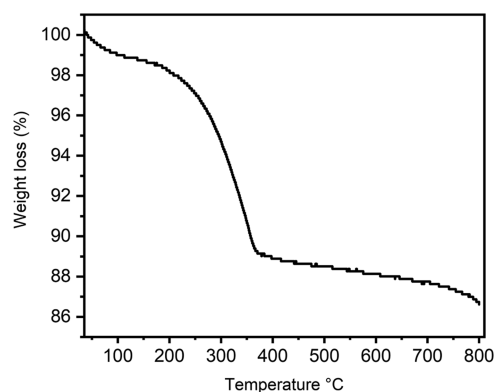

Figure 8. Thermogravimetric analysis (TGA) curve of IONPs synthesized using the *P. Chaba* stem extract (conditions: N_2 and 10 °C/min).

The qualitative analysis of the phytochemicals capped on the surface of IONPs is provided by FTIR, DLS, and EDX. On the other hand, the organic moieties capping the IONPs' surface were quantitatively analyzed by TGA. From the TGA curve (Figure 8), two phases of weight loss were seen. The physisorbed water on the surface of the IONPs evaporates, causing the initial 2% weight loss below 130 °C. The primary cause of the second phase, almost 9% weight loss that occurred at 190−360 °C, is the decomposition of the organic moieties that were capped on the surface of the IONPs.,

2.2. Adsorption Studies. The study of CR adsorption onto the surface of IONPs dispersed in aqueous solvents was performed in batch mode. The adsorption properties of IONPs are strongly dominated by the pH of the solution. Thus, in the

beginning, the effect of pH was investigated on the dye adsorption removal efficiency (*RE*%) in a pH range from 2 to 12 as shown in Figure 9. At constant absorbent mass (20 mg) and initial dye concentration C_0 (20 mg/L), the point charge value of IONPs was found to be 7.05. The positively charged IONPs absorbed the highest amount of negatively charged CR dye at lower pH values. When the pH value increases above the point zero charge, the surface charge of IONPs becomes negative and the electrostatic repulsion induces a desorption of CR. This allows the conclusion that electrostatic interaction is dominant over other possible.[50] The maximum dye adsorption on the IONPs' surface occurred at lower pH, such as pH 2 and 4.
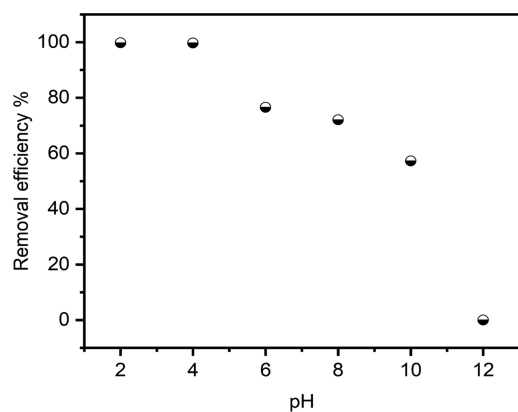
Figure 9. Effect of pH on the adsorption efficiency. $C_0 = 20$ mg/L, $w = 20$ mg, and $v = 0.1$ L.

2.2.1. Kinetics Studies.

The kinetics of adsorption is a crucial component in determining its efficacy. Various kinetic models have been offered by different researchers.[50−54] Three important kinetic models were employed in the current investigation, namely, pseudo-first-order, pseudo-second-order, and intraparticle diffusion (IPD) kinetic models. The time-dependent adsorption of CR was performed at pH 4 using 20 mg/L CR and 20 mg of IONPs in 0.1 L volume. The adsorption of CR was moderately faster within 15 min; after that, the rate was slowed. The adsorption reaches equilibrium in 125 min (Figure 10) with a removal efficiency of 90% and an adsorption capacity of 88 mg/g. Thus, for further study, we fixed the investigation of the adsorption process for 125 min.

The experimental data were fitted to three kinetic models, namely, pseudo-first-order, pseudo-second-order, and IPD kinetics models[54,55] as shown in Figure 11, and the obtained parameters of the adsorption kinetics of CR on IONPs are summarized in Table 1.

The higher correlation coefficients (R^2) above 0.9859 demonstrate that the experimental data are more closely fitted to the pseudo-second-order model (Figure 11 b) than to the pseudo-first-order model (Figure 11a). Further evidence that the adsorption kinetics obeys the pseudo-second-order kinetic model indicates that the adsorption of CR on IONPs is primarily controlled by chemisorption comes from the calculated q_e (cal) values from the pseudo-first-order model (72.44 mg/g), which was lower than the experimental data (88.4 mg/g). On the other hand, the values from the pseudo-

second-order model (95.08 mg/g) agreed well with the experimental data.

Using the intraparticle diffusion (IPD) model developed by Weber and Morris,[56] the mass transport mechanism during dye adsorption onto IONPs is identified. Figure 11c shows the IPD model in its linearized version. The initial portion of the curve makes it evident that dye permeates the solution and adsorbs onto the surface of IONPs. The progressive adsorption shown in the second section of the curve is linked to intraparticle dye diffusion on the IONPs' surface. Pore diffusion is not the only element influencing the rate, though, as evidenced by the line intercept's failure to pass through the origin.

2.2.2. Adsorption Isotherm Studies.

The relationship between the amount of adsorbate absorbed per unit weight of adsorbent (q_e, mg g^{-1}) and the adsorbate concentrations in the bulk solution (C_e, mg L^{-1}) was investigated using adsorption isotherms.[50,54,57] The Langmuir, Freundlich, and Temkin adsorption models, which are frequently used to explain how organic dyes adsorb onto various adsorbents, have been employed, among other adsorption isotherm models.[29,50,52,57−59] The adsorption isotherms of CR onto the surface of IONPs are shown in Figure 12, and the resulting data are presented in Table 2. The weight concentration of IONPs (5−40 mg in 100 mL) and the measurements were carried out at a pH value of 4 for which adsorption is the most efficient. In this case, the amount of IONPs increases with constant concentration of dye until reaching a plateau, which corresponds to the maximum adsorption capacity of IONPs. This maximum is explained by a definite quantity of active sites. In this study, we applied three isotherm models, namely, the Langmuir, Freundlich, and Temkin models.[60] The experimental data are satisfactorily fitted by the Langmuir isotherm model. The C_e/q_e vs C_e plot for the adsorption of CR on IONPs shows a linear relationship with a good correlation coefficient (R^2) of 0.9594. The maximum adsorption capacity (q_m) corresponds to the plateau of the adsorption isotherm, C_e is the concentration of the dye in the solution at equilibrium and K_L is the Langmuir constant. In addition, the Langmuir constant was calculated, and the obtained values were between 0 and 1, indicating a favorable adsorption isotherm. Furthermore, the calculated maximum amount of dye per unit weight of adsorbent value was comparable to the experimental values, indicating the applicability of the Langmuir isotherm model. However, the plots of the Freundlich and Temkin models, typically suitable for systems
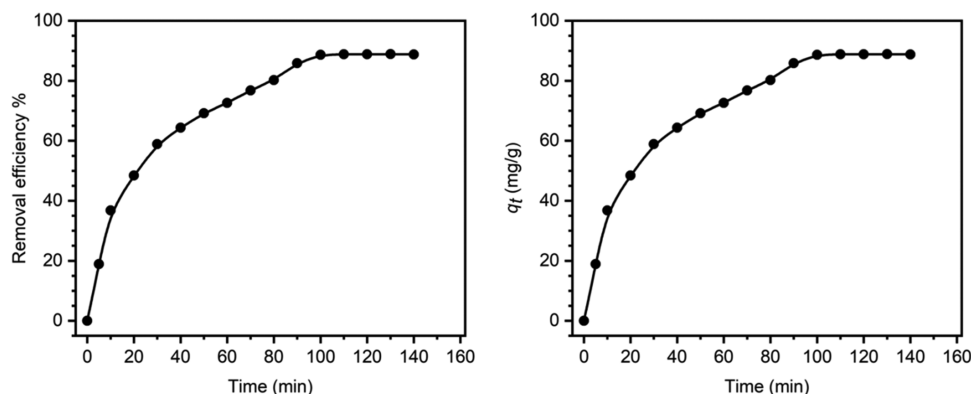

Figure 10. Time dependence of the adsorption of CR onto IONPs. Left-hand side: adsorption capacity and right-hand side: removal efficiency (condition: $C_{CR0} = 20$ mg/L, $V = 100$ mL, and $W_{IONPs} = 20$ mg).
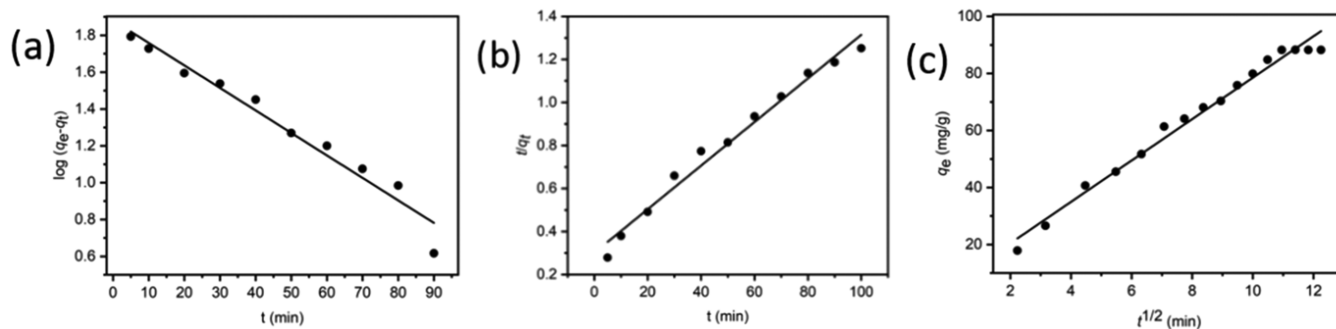
Figure 11. Fitted plots of (a) pseudo-first-order, (b) pseudo-second-order, and (c) IPD kinetics model for the adsorption of CR on IONPs.

Table 1. Parameters Obtained from Kinetic Models for CR Adsorption on IONPs

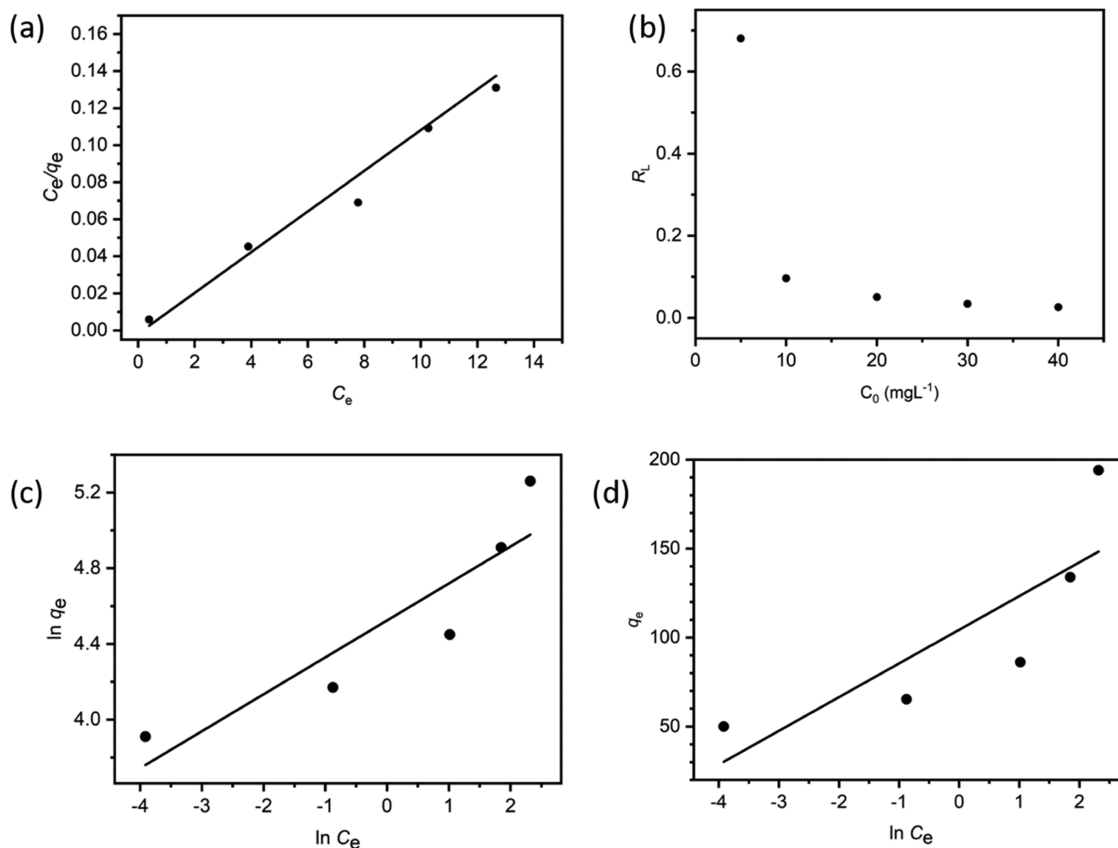| model and equations	parameters			
	K_1 (×10^{-4}/min)	q_{cal} (mg/g)	q_{exp} (mg/g)	R^2
pseudo−first order	1.35	72.44	88.4	0.9505
$\log(q_e - q_t) = \log q_e - \frac{k_1}{2.303}t$				
	K_2 (×10^{-4} g/(mg·min))	q_{cal} (mg/g)	q_{exp} (mg/g)	R^2
pseudo-second order	3.51	95.08	88.4	0.9859
$\frac{t}{q_t} = \frac{1}{k_2 q_e^2} + \frac{t}{q_t}$				
	k_{dif} (mg/(g·min$^{1/2}$))	R_i	C (mg/g)	R^2
intraparticle diffusion	7.26	0.93	5.89	0.9728
$q_t = k_{dif} t^{1/2} + C$				
$R_i = \frac{q_{ref} - C}{q_{ref}}$				

Figure 12. Fitted plots for (a) Langmuir, (b) R_L vs C_0, (c) Freundlich, and (d) Temkin isotherm model for the adsorption of CR on IONPs.

Table 2. Constant Parameters and Correlation Coefficients Calculated for Different Adsorption Isotherm Models for CR Adsorption on IONPs

| model and equations	constants	
Langmuir	q_m (mg/g)	108.10
	R_L ($C_0 = 5$ mg/L)	0.6802
	$C_0 = 10$ mg/L	0.0961
	$C_0 = 20$ mg/L	0.0505
$\frac{C_e}{q_e} = \frac{1}{q_m b} + \frac{C_e}{q_m}$; $R_L = \frac{1}{1 + bC_0}$	$C_0 = 30$ mg/L	0.0342
	$C_0 = 40$ mg/L	0.0259
	b (L/mg)	0.94
	R^2	**0.9726**
Freundlich	n	0.2369
$\ln q_e = \ln KF + \frac{1}{n} \ln C_e$	K_F (mg/g(L/mg)$^{1/n}$)	51.70
	R^2	**0.7650**
Temkin	b_T	67.71
	A_T (L/g)	36.59
$q_e = B \ln A_T + B \ln C_e$; considering $B = \frac{RT}{b_T}$	B (J/mol)	83.45
	R^2	**0.5702**

with heterogeneous surface and adsorption-adsorption interactions, respectively, are not linear with low R^2 values.

It is quite difficult to make a comparison because there has been little research on CR adsorption on green synthesized IONPs. Finally, take note of the fact that the maximum adsorption capacity for CR was determined to be 88 mg/g in this work that is higher than magnetite iron oxide kaolinite nanocomposite for a maximum adsorption capacity of 45.59 mg/g,[61] guar gum-coated iron oxide nanocomposite of 62.24 mg/g,[62] M-cell/Fe$_3$O$_4$/ACCs of 66.09 mg/g,[63] and comparable with iron oxide-BC of 104.17 mg/g,[58] and lower than amine-functionalized magnetite IONP of 183 mg/g.[64] Although amorphous iron nanoparticles offer a higher adsorption capacity of 1735 mg/g for CR, the IONPs synthesized in this work could be a prominent adsorbent for CR removal.

The adsorptive process can be directly impacted by pH since the adsorption processes are often characterized by $\pi-\pi$ interactions, hydrogen bonding, electrostatic interactions, and pore/size-selective adsorption.[50,58] The adsorption process in this work was carried out at pH 4, which resulted in the surface of the IONPs being positively charged. However, intraparticle diffusion (IPD) is not the rate-determining step of this adsorption process; therefore, the electrostatic interaction between the positive surface of IONPs and SO$_3^-$ ions of CR as well as the hydrogen bonds between different phytochemicals on the IONPs surface and NH$_2$ groups of CR might be considered the probable interaction among IONPs and CR. A similar adsorption mechanism was also proposed for the adsorption of CR onto IONPs in the reported work.[58]

2.2.3. Effect of Adsorbent Dosage. The maximum efficiency of the adsorptions of CR over IONPs was investigated using different amounts of IONPs (5 to 40 mg) at a fixed CR concentration (20 mg/L). The effect of different amounts of the IONPs on the adsorption of CR is shown in Figure 13. The removal efficiency of CR increased from 48 to 100% by increasing the amount of IONPs from 5 to 40 mg due to increasing adsorption sites. However, the adsorption capacity decreased from 194 to 59 mg/g as the mass of IONPs increased from 5 to 40 mg due to the increase in the unutilized adsorption sites.

2.2.4. Effect of the Initial Dye Concentration. The effect of the initial concentration of CR dye on the adsorption onto
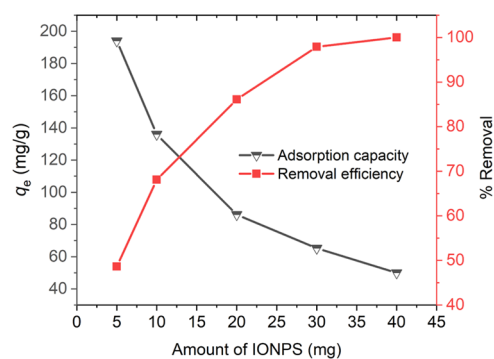
Figure 13. Effect of the dosage of IONPs on the adsorption process ($C_{CR} = 20$ mg/L and $V = 100$ mL).

IONPs is shown in Figure 14. The experiment was carried out using 10 mg of IONP absorbent using 5 to 25 mg/L of CR in
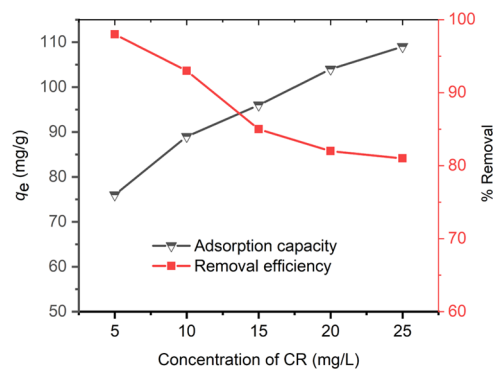
Figure 14. Effect of the initial concentration of CR on the adsorption process ($W_{IONPS} = 10$ mg, $V = 100$ mL).

100 mL solution. The dye removal efficiency of the IONPs decreased with an increase in the CR concentration. The CR removal efficiency decreased from 98 to 81%. At lower concentrations of CR, a sufficient amount of IONPs leads to more active sites available for adsorption and causes higher efficiency. On the other hand, higher concentration CR leads to saturated active sites, resulting in lower dye removal efficiency despite the increasing of q_e. The effect of the initial

adsorbate concentration on adsorption has been well studied and reveals that concentration and adsorption efficiency are inversely related, which also funds CR absorption on IONPs.

2.2.5. Reusability. The reusability of dye adsorbents is one of the key factors for evaluating the performance. The reusability performance was investigated by five successive adsorption/desorption cycles using an initial concentration of 20 mg/L of 100 mL of CR solution with 10 mg of IONPs. Adsorption was performed at pH = 4 and desorption was performed at pH = 12 using hydrochloric acid and sodium hydroxide to maintain the pH. Figure 15 shows that during the
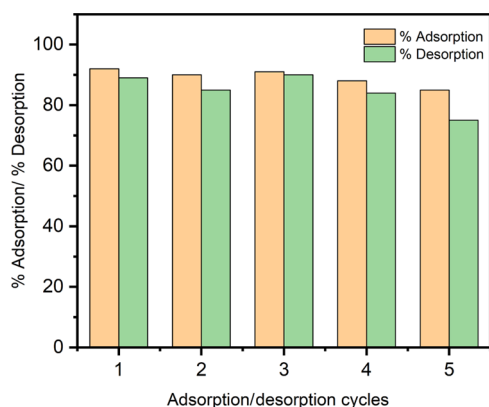

Figure 15. Recycling performance of IONPs for capturing CR up to 5 cycles.

first to fifth cycles the quantity of CR adsorbed ranged from 92 to 85%, whereas the quantities of CR desorption varied within the same cycle from 89 to 75%. The slight decrease in adsorption might have resulted from both partial CR desorption and the loss of a trace amount of IONPs during washing. Conversely, a shorter desorption time might have resulted from the application of less time for the desorption process. Nonetheless, it could be claimed that IONPs' notable reusability indicates their potential for removing different types of dyes during wastewater treatment.

3. EXPERIMENTAL SECTION

3.1. Chemicals. Analytical grade ferrous sulfate heptahydrate, ferric chloride, sodium hydroxide, hydrochloric acid, and congo red were purchased from Merck India and used without any prior purification. Stock solutions of dye were obtained by dissolving the powder in deionized water, followed by an orbital shaker stirring for 30 min. All of the reagents were used directly without further purification. Deionized water was used throughout the study.

3.2. Collection of Plant Materials. The stem of *P. chaba* was freshly collected from Gollamari Bazar, Khulna District, Bangladesh. The stem was thoroughly washed with deionized distilled water, cut into small pieces, and air-dried at room temperature.

3.3. Preparation of Plant Extract. Finely cut stems (approximately 30 g) were placed in a round-bottomed flask containing deionized distilled water (200 mL) and boiled for 40 min. The extract was cooled, filtered using filter paper, and stored at 4 °C for further use.

3.4. Synthesis of IONPs. The IONPs were synthesized according to the literature with slight modifications.[65,66] Ferric chloride and ferrous sulfate heptahydrate were mixed in a 2:1

ratio in water. The yellow solution mixture was heated to 80 °C for 30 min. Then, 1 mL of extract was added dropwise and continued heat for another 1 h. Following this, 1 M NaOH was added dropwise until pH reached 11 and heat continued for another 15 min. At this time, black precipitation was observed from the brown solution mixture. Finally, magnetite IONPs were washed with distilled water several times and adjusted to pH 7. The resulting IONPs were vacuum-dried at 60 °C for 24 h and stored for further study.

3.5. Measurements. UV−vis spectroscopic analysis was carried out on a SHIMADZU UV-1900i UV−vis spectrophotometer. Absorption spectra were recorded at a resolution of 1 nm within 200−800 nm. The hydrodynamic size was measured through DLS analysis conducted on a Malvern (Malvern, UK) Zetasizer Nano ZS instrument. FTIR spectra were recorded on a SHIMADZU (Tokyo, Japan) IRSpirit Fourier transform infrared spectrophotometer using a KBr pellet with a scan rate of approximately 4 cm^{-1} s^{-1} at 25 °C. SEM measurements and EDX analysis were conducted on a Hitachi SU-8000 microscope at accelerating voltages of 10 and 15 kV. TEM measurements were conducted on a TEM-2100F (JEOL, Tokyo, Japan) field emission electron microscope. XRD analysis was conducted on a Rigaku SmartLab spectrometer with Cu-Kα radiation. Magnetic behavior was examined by a VSM 8604, Lakeshore Crytronics Inc., USA at room temperature. TGA was carried out on a SHIMADZU (Tokyo, Japan) TGA-50 at a heating rate of 10 °C min^{-1} under N$_2$.

3.6. Zero-Point Charge (ZPC). Zero-point charge (ZPC) is the pH of a solution at which the net charge on the surface of IONPs becomes neutral (pHzpc). This was measured by the well-established pH drift method.[67] 15 mL of 4 mM sodium chloride was taken in a specific number of containers, and the pH was adjusted using 1 M NaOH or 1 M HCl acid between 2 and 12 with increments of 1. To all of the beakers, 20 mg of IONPs was added and kept at room temperature for 48 h for the stabilization of pH. Each beaker's final pH was measured after 24 h, and the initial pH and the difference between the initial and final pH values were used to display the results on a graph. Now, the intersection of this curve where it crosses the initial pH and the difference between the initial and final pH lines is known as pH$_{zpc}$.

3.7. Adsorption of CR on IONPs. Batch adsorption experiments were carried out at room temperature to evaluate the adsorption kinetics and the effect of pH (batch test). Adsorption of CR was carried out by adding 20 mg of IONPs into 100 mL of 20 mg/L CR solution in Erlenmeyer flasks. The resulting mixture was stirred at 200 rpm using a shaker for up to 3 h at different pH (2, 3, 4, 5, 6, 7, 8, 9, 10, 11, and 12) to optimize the pH. At the specific time, IONPs were precipitated by centrifugation at 10,000 rpm for 4 min, and the final concentration of CR in the supernatant was determined from optical absorption at 498 nm.

After optimizing the pH value at 4, the effect of the contact time (batch) experiment was carried out by adding 20 mg of IONPs into 100 mL of 20 mg/L CR solution for the adsorption kinetics study. Similarly, adsorption isotherm was obtained by batch experiments by adding 20 mg of IONPs in 100 mL of CR solution with different concentrations in the range of 5−100 mg/L. The dependence of removal of CR on the mass of IONPs was determined by using different adding masses of IONPs (20−100 mg) into a series of Erlenmeyer flasks, which contain 100 mL of 20 mg IONP solution.

The adsorption capacity (q_t, the amount of adsorbed CR per unit mass of adsorbent) of IONPs was calculated by the following equation[68]

$$q_t = \frac{(C_0 - C_t)V}{W} \tag{2}$$

where C_0 and C_t are the concentrations (mg/L) of CR at initial and at time t, respectively; V represents the volume of the solution (L); W is the adsorbent mass (g). C_e (mg/L) and q_e denote the equilibrium concentration and equilibrium adsorption capacity, respectively. The removal efficiency (RE %) was calculated by the following equation[69]

$$\text{RE\%} = \frac{(C_0 - C_e)}{C_0} \times 100 \tag{3}$$

4. CONCLUSIONS

In summary, we successfully synthesized magnetite IONPS via a green approach utilizing *P. chaba* stem extract as reducing and capping agents. Spectroscopic methods and DLS and TG analysis validate the formation of stable IONPs capped by organic moieties derived from *P. chaba* stem extract. The formation of spherical IONPs with a crystalline nature and an average size of 9 nm was confirmed by XRD, SEM, and TEM analyses. In addition, the produced IONPs have a superparamagnetic nature confirmed by VSM measurement. The point charge value of IONPs was 7.05, indicating that positively charged IONPs can adsorb the highest amount of negatively charged dye. Using Congo red (CR) as a model, the use of the resulting IONPs as an adsorbent for organic contaminants was examined. The isotherm and kinetics analysis demonstrated that chemisorption and the development of a monolayer on the homogeneous IONPs' surface via adsorbate−adsorbent interaction were responsible for the adsorption of CR onto IONPs. Overall, as it is safer and less harmful to the environment than chemical approaches, simple green synthesis of IONPs may be an expectative alternative and obtained IONPs may also be used for a variety of applications.

■ AUTHOR INFORMATION

Corresponding Author

  Habib Md. Ahsan − *Chemistry Discipline, Khulna University, Khulna 9208, Bangladesh;* orcid.org/0000-0003-0311-425X; Email: ahsanhru@chem.ku.ac.bd

Authors

  Sangjukta Yesmin − *Chemistry Discipline, Khulna University, Khulna 9208, Bangladesh*

  Md. Mahiuddin − *Chemistry Discipline, Khulna University, Khulna 9208, Bangladesh;* orcid.org/0000-0002-1195-9159

  A. B. M. Nazmul Islam − *Chemistry Discipline, Khulna University, Khulna 9208, Bangladesh*

  Kaykobad Md Rezaul Karim − *Chemistry Discipline, Khulna University, Khulna 9208, Bangladesh*

  Prianka Saha − *Chemistry Discipline, Khulna University, Khulna 9208, Bangladesh*

  Md. Abu Rayhan Khan − *Chemistry Discipline, Khulna University, Khulna 9208, Bangladesh*

Complete contact information is available at:
https://pubs.acs.org/10.1021/acsomega.3c09557

Author Contributions

This work was conducted by all authors.

Notes

The authors declare no competing financial interest.

■ ACKNOWLEDGMENTS

■ REFERENCES

(1) Desireddy, A.; Conn, B. E.; Guo, J.; Yoon, B.; Barnett, R. N.; Monahan, B. M.; Kirschbaum, K.; Griffith, W. P.; Whetten, R. L.; Landman, U.; Bigioni, T. P. Ultrastable Silver Nanoparticles. *Nature* **2013**, *501* (7467), 399−402.

(2) Njagi, E. C.; Huang, H.; Stafford, L.; Genuino, H.; Galindo, H. M.; Collins, J. B.; Hoag, G. E.; Suib, S. L. Biosynthesis of Iron and Silver Nanoparticles at Room Temperature Using Aqueous Sorghum Bran Extracts. *Langmuir* **2011**, *27* (1), 264−271.

(3) Raveendran, P.; Fu, J.; Wallen, S. L. Completely "Green" Synthesis and Stabilization of Metal Nanoparticles. *J. Am. Chem. Soc.* **2003**, *125* (46), 13940−13941.

(4) Darr, J. A.; Zhang, J.; Makwana, N. M.; Weng, X. Continuous Hydrothermal Synthesis of Inorganic Nanoparticles: Applications and Future Directions. *Chem. Rev.* **2017**, *117* (17), 11125−11238.

(5) Sui, R.; Charpentier, P. Synthesis of Metal Oxide Nanostructures by Direct Sol−Gel Chemistry in Supercritical Fluids. *Chem. Rev.* **2012**, *112* (6), 3057−3082.

(6) Negrescu, A. M.; Killian, M. S.; Raghu, S. N. V.; Schmuki, P.; Mazare, A.; Cimpean, A. Metal Oxide Nanoparticles: Review of Synthesis, Characterization and Biological Effects. *J. Funct. Biomater.* **2022**, *13* (4), 274.

(7) Yoon, Y.; Truong, P. L.; Lee, D.; Ko, S. H. Metal-Oxide Nanomaterials Synthesis and Applications in Flexible and Wearable Sensors. *ACS Nanosci. Au* **2022**, *2* (2), 64−92.

(8) Singh, J.; Dutta, T.; Kim, K.-H.; Rawat, M.; Samddar, P.; Kumar, P. Green' Synthesis of Metals and Their Oxide Nanoparticles: Applications for Environmental Remediation. *J. Nanobiotechnol.* **2018**, *16* (1), 84.

(9) Laurent, S.; Forge, D.; Port, M.; Roch, A.; Robic, C.; Vander Elst, L.; Muller, R. N. Magnetic Iron Oxide Nanoparticles: Synthesis, Stabilization, Vectorization, Physicochemical Characterizations, and Biological Applications. *Chem. Rev.* **2008**, *108* (6), 2064−2110.

(10) Ali, A.; Zafar, H.; Zia, M.; ul Haq, I.; Phull, A. R.; Ali, J. S.; Hussain, A. Synthesis, Characterization, Applications, and Challenges of Iron Oxide Nanoparticles. *Nanotechnol. Sci. Appl.* **2016**, *9*, 49−67.

(11) Chavali, M. S.; Nikolova, M. P. Metal Oxide Nanoparticles and Their Applications in Nanotechnology. *SN Appl. Sci.* **2019**, *1* (6), No. 607.

(12) Wu, W.; He, Q.; Jiang, C. Magnetic Iron Oxide Nanoparticles: Synthesis and Surface Functionalization Strategies. *Nanoscale Res. Lett.* **2008**, *3* (11), 397.

(13) Ge, S.; Shi, X.; Sun, K.; Li, C.; Uher, C.; Baker, J. R.; Banaszak Holl, M. M.; Orr, B. G. Facile Hydrothermal Synthesis of Iron Oxide Nanoparticles with Tunable Magnetic Properties. *J. Phys. Chem. C* **2009**, *113* (31), 13593−13599.

(14) Babes, L.; Denizot, B.; Tanguy, G.; Le Jeune, J. J.; Jallet, P. Synthesis of Iron Oxide Nanoparticles Used as MRI Contrast Agents: A Parametric Study. *J. Colloid Interface Sci.* **1999**, *212* (2), 474−482.

(15) Samrot, A. V.; Sahithya, C. S.; Selvarani A, J.; Purayil, S. K.; Ponnaiah, P. A Review on Synthesis, Characterization and Potential Biological Applications of Superparamagnetic Iron Oxide Nanoparticles. *Curr. Res. Green Sustainable Chem.* **2021**, *4* (November 2020), No. 100042.

(16) Hassanjani-Roshan, A.; Vaezi, M. R.; Shokuhfar, A.; Rajabali, Z. Synthesis of Iron Oxide Nanoparticles via Sonochemical Method and Their Characterization. *Particuology* **2011**, *9* (1), 95−99.

(17) Kostyukova, D.; Chung, Y. H. Synthesis of Iron Oxide Nanoparticles Using Isobutanol. *J. Nanomater.* **2016**, *2016* (Ii), 1−9.

(18) Win, T. T.; Khan, S.; Bo, B.; Zada, S.; Fu, P. Green Synthesis and Characterization of Fe3O4 Nanoparticles Using Chlorella-K01 Extract for Potential Enhancement of Plant Growth Stimulating and Antifungal Activity. *Sci. Rep.* **2021**, *11* (1), No. 21996.

(19) Lakshminarayanan, S.; Shereen, M. F.; Niraimathi, K. L.; Brindha, P.; Arumugam, A. One-Pot Green Synthesis of Iron Oxide Nanoparticles from Bauhinia Tomentosa: Characterization and Application towards Synthesis of 1, 3 Diolein. *Sci. Rep.* **2021**, *11* (1), No. 8643.

(20) Saif, S.; Tahir, A.; Chen, Y. Green Synthesis of Iron Nanoparticles and Their Environmental Applications and Implications. *Nanomaterials* **2016**, *6* (11), 209.

(21) Batool, F.; Iqbal, M. S.; Khan, S.-U.-D.; Khan, J.; Ahmed, B.; Qadir, M. I. Biologically Synthesized Iron Nanoparticles (FeNPs) from Phoenix Dactylifera Have Anti-Bacterial Activities. *Sci. Rep.* **2021**, *11* (1), No. 22132.

(22) Hao, R.; Li, D.; Zhang, J.; Jiao, T. Green Synthesis of Iron Nanoparticles Using Green Tea and Its Removal of Hexavalent Chromium. *Nanomaterials* **2021**, *11* (3), 650.

(23) AL-Husseini, A. H.; Sih, B. T.; Al-Araji, A. M. Green Synthesis of Iron Oxide Nanoparticles (Fe 2 O 3) Using Saffron Extract. *J. Phys. Conf. Ser.* **2021**, *2114* (1), No. 012082.

(24) Andrade-Zavaleta, K.; Chacon-Laiza, Y.; Asmat-Campos, D.; Raquel-Checca, N. Green Synthesis of Superparamagnetic Iron Oxide Nanoparticles with Eucalyptus Globulus Extract and Their Application in the Removal of Heavy Metals from Agricultural Soil. *Molecules* **2022**, *27* (4), 1367.

(25) Adhikari, A.; Chhetri, K.; Acharya, D.; Pant, B.; Adhikari, A. Green Synthesis of Iron Oxide Nanoparticles Using Psidium Guajava L. Leaves Extract for Degradation of Organic Dyes and Anti-Microbial Applications. *Catalysts* **2022**, *12* (10), 1188.

(26) Ebrahiminezhad, A.; Zare-Hoseinabadi, A.; Sarmah, A. K.; Taghizadeh, S.; Ghasemi, Y.; Berenjian, A. Plant-Mediated Synthesis and Applications of Iron Nanoparticles. *Mol. Biotechnol.* **2018**, *60* (2), 154−168.

(27) Beheshtkhoo, N.; Kouhbanani, M. A. J.; Savardashtaki, A.; Amani, A. M.; Taghizadeh, S. Green Synthesis of Iron Oxide Nanoparticles by Aqueous Leaf Extract of Daphne Mezereum as a Novel Dye Removing Material. *Appl. Phys. A: Mater. Sci. Process.* **2018**, *124* (5), No. 363.

(28) Abid, M. A.; Kadhim, D. A.; Aziz, W. J. Iron Oxide Nanoparticle Synthesis Using Trigonella and Tomato Extracts and Their Antibacterial Activity. *Mater. Technol.* **2022**, *37* (8), 547−554.

(29) Anwer, Z.; Jamali, A. R.; Khan, W.; Bhatti, J.; Akhter, F.; Batool, M. Green Synthesis of Active Fe2O3 Nanoparticles Using Aloe Barbadensis and Camellia Sinensis for Efficient Degradation of Malachite Green and Congo Red Dye *Biomass Convers. Biorefin.* **2022**, DOI: 10.1007/s13399-022-03626-3.

(30) Razack, S. A.; Suresh, A.; Sriram, S.; Ramakrishnan, G.; Sadanandham, S.; Veerasamy, M.; Nagalamadaka, R. B.; Sahadevan, R. Green Synthesis of Iron Oxide Nanoparticles Using Hibiscus Rosa-Sinensis for Fortifying Wheat Biscuits. *SN Appl. Sci.* **2020**, *2* (5), No. 898.

(31) de Lima Barizão, A. C.; Silva, M. F.; Andrade, M.; Brito, F. C.; Gomes, R. G.; Bergamasco, R. Green Synthesis of Iron Oxide Nanoparticles for Tartrazine and Bordeaux Red Dye Removal. *J. Environ. Chem. Eng.* **2020**, *8* (1), No. 103618.

(32) Chauhan, S.; Kumar, D. N.; Upadhyay, L. S. B. Facile Synthesis of Iron Oxide Nanoparticles Using Lawsonia Inermis Extract and Its Application in Decolorization of Dye. *Bionanoscience* **2019**, *9* (4), 789−798.

(33) Ting, A. S. Y.; Chin, J. E. Biogenic Synthesis of Iron Nanoparticles from Apple Peel Extracts for Decolorization of Malachite Green Dye. *Water, Air, Soil Pollut.* **2020**, *231* (6), No. 278.

(34) Bhuiyan, M. S. H.; Miah, M. Y.; Paul, S. C.; Aka, T. Das.; Saha, O.; Rahaman, M. M.; Sharif, M. J. I.; Habiba, O.; Ashaduzzaman, M. Green Synthesis of Iron Oxide Nanoparticle Using Carica Papaya Leaf Extract: Application for Photocatalytic Degradation of Remazol Yellow RR Dye and Antibacterial Activity. *Heliyon* **2020**, *6* (8), No. e04603.

(35) Taufiq-Ur-Rahman, M.; Ahmad Shilpi, J.; Ahmed, M.; Faiz Hossain, C. Preliminary Pharmacological Studies on *Piper Chaba* Stem Bark. *J. Ethnopharmacol.* **2005**, *99* (2), 203−209.

(36) Rao, V. R. S.; Suresh, G.; Babu, K. S.; Raju, S. S.; Vishnu vardhan, M. V. P. S.; Ramakrishna, S.; Rao, J. M. Novel Dimeric Amide Alkaloids from *Piper Chaba* Hunter: Isolation, Cytotoxic Activity, and Their Biomimetic Synthesis. *Tetrahedron* **2011**, *67* (10), 1885−1892.

(37) Bhandari, S. P. S.; Babu, U. V.; Garg, Late. H.S. A Lignan from *Piper Chaba* Stems. *Phytochemistry* **1998**, *47* (7), 1435−1436.

(38) Naz, T.; Mosaddik, A.; Rahman, M. M.; Muhammad, I.; Haque, M. E.; Cho, S. K. Antimicrobial, Antileishmanial and Cytotoxic Compounds from *Piper Chaba*. *Nat. Prod. Res.* **2012**, *26* (11), 979−986.

(39) Mahiuddin, M.; Saha, P.; Ochiai, B. Green Synthesis and Catalytic Activity of Silver Nanoparticles Based on *Piper Chaba* Stem Extracts. *Nanomaterials* **2020**, *10* (9), 1777.

(40) Kumar, B. Green Synthesis of Gold, Silver, and Iron Nanoparticles for the Degradation of Organic Pollutants in Wastewater. *J. Compos. Sci.* **2021**, *5* (8), 219.

(41) Lohrasbi, S.; Kouhbanani, M. A. J.; Beheshtkhoo, N.; Ghasemi, Y.; Amani, A. M.; Taghizadeh, S. Green Synthesis of Iron Nanoparticles Using Plantago Major Leaf Extract and Their Application as a Catalyst for the Decolorization of Azo Dye. *Bionanoscience* **2019**, *9* (2), 317−322.

(42) Ahsani-Namin, Z.; Norouzbeigi, R.; Shayesteh, H. Green Mediated Combustion Synthesis of Copper Zinc Oxide Using Eryngium Planum Leaf Extract as a Natural Green Fuel: Excellent Adsorption Capacity towards Congo Red Dye. *Ceram. Int.* **2022**, *48* (14), 20961−20973.

(43) Hossan, M.; Ochiai, B. Preparation of TiO2-Poly(3-Chloro-2-Hydroxypropyl Methacrylate) Nanocomposite for Selective Adsorption and Degradation of Dyes. *Technologies* **2018**, *6* (4), 92.

(44) Firdaus, R. M.; Rosli, N. I. M.; Ghanbaja, J.; Vigolo, B.; Mohamed, A. R. Enhanced Adsorption of Methylene Blue on Chemically Modified Graphene Nanoplatelets Thanks to Favorable Interactions. *J. Nanopart. Res.* **2019**, *21* (12), No. 257.

(45) Alhalili, Z. Green Synthesis of Copper Oxide Nanoparticles CuO NPs from Eucalyptus Globoulus Leaf Extract: Adsorption and Design of Experiments. *Arabian J. Chem.* **2022**, *15* (5), No. 103739.

(46) Mahdavi, M.; Namvar, F.; Ahmad, M.; Mohamad, R. Green Biosynthesis and Characterization of Magnetic Iron Oxide (Fe3O4) Nanoparticles Using Seaweed (Sargassum Muticum) Aqueous Extract. *Molecules* **2013**, *18* (5), 5954−5964.

(47) V G, V. K.; A Prem, A. Green Synthesis and Characterization of Iron Oxide Nanoparticles Using Phyllanthus Niruri Extract. *Orient. J. Chem.* **2018**, *34* (5), 2583−2589.

(48) Rukachaisirikul, T.; Prabpai, S.; Champung, P.; Suksamrarn, A. Chabamide, a Novel Piperine Dimer from Stems of *Piper Chaba*. *Planta Med.* **2002**, *68* (9), 853−855.

(49) Mandal Bis, S.; Chakrabort, N.; Chakrabort, P.; Sarkar, S. Antioxidant and Antimicrobial Activities of the Hot Pungent Chabbarin Are Responsible for the Medicinal Properties of *Piper Chaba*, Hunter. *Res. J. Med. Plant* **2012**, *6* (8), 574−586.

(50) Talbot, D.; Queiros Campos, J.; Checa-Fernandez, B. L.; Marins, J. A.; Lomenech, C.; Hurel, C.; Godeau, G. D.; Raboisson-Michel, M.; Verger-Dubois, G.; Obeid, L.; et al. Adsorption of Organic Dyes on Magnetic Iron Oxide Nanoparticles. Part I: Mechanisms and Adsorption-Induced Nanoparticle Agglomeration. *ACS Omega* **2021**, *6* (29), 19086−19098.

(51) Nodehi, R.; Shayesteh, H.; Kelishami, A. R. Enhanced Adsorption of Congo Red Using Cationic Surfactant Functionalized Zeolite Particles. *Microchem. J.* **2020**, *153*, No. 104281.

(52) Islam, A. B. M. N.; Saha, P.; Hossain, M. E.; Habib, M. A.; Karim, K. M. R.; Mahiuddin, M. Green Coffee Bean Extract Assisted Facile Synthesis of Reduced Graphene Oxide and Its Dye Removal Activity. *Global Challenges* **2023**, *8* (1), No. 2300247.

(53) Mahiuddin, M.; Ochiai, B. Lemon Juice Assisted Green Synthesis of Reduced Graphene Oxide and Its Application for Adsorption of Methylene Blue. *Technologies* **2021**, *9* (4), 96.

(54) Kim, S.-H.; Choi, P.-P. Enhanced Congo Red Dye Removal from Aqueous Solutions Using Iron Nanoparticles: Adsorption, Kinetics, and Equilibrium Studies. *Dalton Trans.* **2017**, *46* (44), 15470−15479.

(55) Lei, C.; Zhu, X.; Zhu, B.; Yu, J.; Ho, W. Hierarchical NiO−SiO2 Composite Hollow Microspheres with Enhanced Adsorption Affinity towards Congo Red in Water. *J. Colloid Interface Sci.* **2016**, *466*, 238−246.

(56) Boyd, G. E.; Schubert, J.; Adamson, A. W. The Exchange Adsorption of Ions from Aqueous Solutions by Organic Zeolites. I. Ion-Exchange Equilibria 1. *J. Am. Chem. Soc.* **1947**, *69* (11), 2818−2829.

(57) Nethaji, S.; Sivasamy, A.; Mandal, A. B. Adsorption Isotherms, Kinetics and Mechanism for the Adsorption of Cationic and Anionic Dyes onto Carbonaceous Particles Prepared from Juglans Regia Shell Biomass. *Int. J. Environ. Sci. Technol.* **2013**, *10* (2), 231−242.

(58) Borth, K. W.; Galdino, C. W.; Teixeira, V. de C.; Anaissi, F. J. Iron Oxide Nanoparticles Obtained from Steel Waste Recycling as a Green Alternative for Congo Red Dye Fast Adsorption. *Appl. Surf. Sci.* **2021**, *546* (July 2020), No. 149126.

(59) Al-Ghouti, M. A.; Al-Absi, R. S. Mechanistic Understanding of the Adsorption and Thermodynamic Aspects of Cationic Methylene Blue Dye onto Cellulosic Olive Stones Biomass from Wastewater. *Sci. Rep.* **2020**, *10* (1), No. 15928.

(60) Foo, K. Y.; Hameed, B. H. Insights into the Modeling of Adsorption Isotherm Systems. *Chem. Eng. J.* **2010**, *156* (1), 2−10.

(61) Mahmud, N.; Benamor, A. Magnetic Iron Oxide Kaolinite Nanocomposite for Effective Removal of Congo Red Dye: Adsorption, Kinetics, and Thermodynamics Studies. *Water Conserv. Sci. Eng.* **2023**, *8* (1), No. 35.

(62) Sahoo, J. K.; Kumar, A.; Rath, J.; Mohanty, T.; Dash, P.; Sahoo, H. Guar Gum-Coated Iron Oxide Nanocomposite as an Efficient Adsorbent for Congo Red Dye. *Desalin. Water Treat.* **2017**, *95*, 342−354.

(63) Zhu, H.-Y.; Fu, Y.-Q.; Jiang, R.; Jiang, J.-H.; Xiao, L.; Zeng, G.-M.; Zhao, S.-L.; Wang, Y. Adsorption Removal of Congo Red onto Magnetic Cellulose/Fe$_3$O$_4$/Activated Carbon Composite: Equilibrium, Kinetic and Thermodynamic Studies. *Chem. Eng. J.* **2011**, *173* (2), 494−502.

(64) Sahoo, J. K.; Paikra, S. K.; Mishra, M.; Sahoo, H. Amine Functionalized Magnetic Iron Oxide Nanoparticles: Synthesis, Antibacterial Activity and Rapid Removal of Congo Red Dye. *J. Mol. Liq.* **2019**, *282*, 428−440.

(65) Ali, I. New Generation Adsorbents for Water Treatment. *Chem. Rev.* **2012**, *112* (10), 5073−5091.

(66) M Awwad, A.; M Salem, N. A Green and Facile Approach for Synthesis of Magnetite Nanoparticles. *Nanosci. Nanotechnol.* **2012**, *2* (6), 208−213.

(67) Kulkarni, S. D.; Kumbar, S.; Menon, S. G.; Choudhari, K. S.; C, S. Magnetically Separable Core−Shell ZnFe$_2$O$_4$@ZnO Nanoparticles for Visible Light Photodegradation of Methyl Orange. *Mater. Res. Bull.* **2016**, *77*, 70−77.

(68) Arias Arias, F.; Guevara, M.; Tene, T.; Angamarca, P.; Molina, R.; Valarezo, A.; Salguero, O.; Vacacela Gomez, C.; Arias, M.; Caputi, L. S. The Adsorption of Methylene Blue on Eco-Friendly Reduced Graphene Oxide. *Nanomaterials* **2020**, *10* (4), 681.

(69) Poudel, M. B.; Yu, C.; Kim, H. J. Synthesis of Conducting Bifunctional Polyaniline@Mn-TiO$_2$ Nanocomposites for Supercapacitor Electrode and Visible Light Driven Photocatalysis. *Catalysts* **2020**, *10* (5), 546.